# Supporting Information

## A Bio-inspired Electrocatalyst for Electrochemical Reduction of $N_2$ to $NH_3$ at Ambient Conditions

Haohong Xian,[†] Haoran Guo,[¶] Zhishu Chen,[†] Guangsen Yu, [†] Abdulmohsen Ali Alshehri, [§] Khalid Ahmed Alzahrani,[§] Feng Hao,[†] Rui Song[*,¶] and Tingshuai Li[*,†]

† School of Materials and Energy, University of Electronic Science and Technology of China, Chengdu 611731, Sichuan, China

¶ School of Chemical Sciences, University of Chinese Academy of Sciences, 19 Yuquan Road, Shijingshan District, Beijing, 100049, China

§ Chemical Synthesis and Pollution Control, Key Laboratory of Sichuan Province, School of Chemistry and Chemical engineering, China West Normal University, Nanchong, 6337002, Sichuan, China

*E-mails: rsong@ucas.ac.cn and litingshuai@uestc.edu.cn

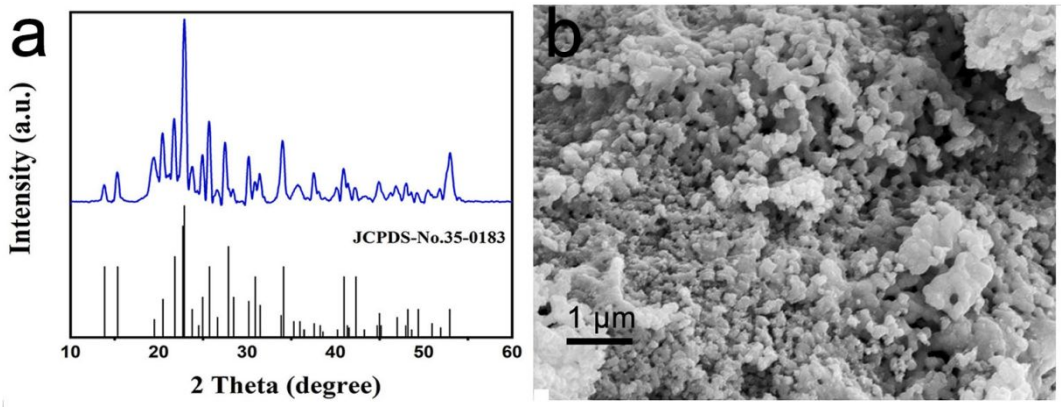


**Fig. S1**. (a) XRD pattern and (b) SEM of the FMO-NPs sample.

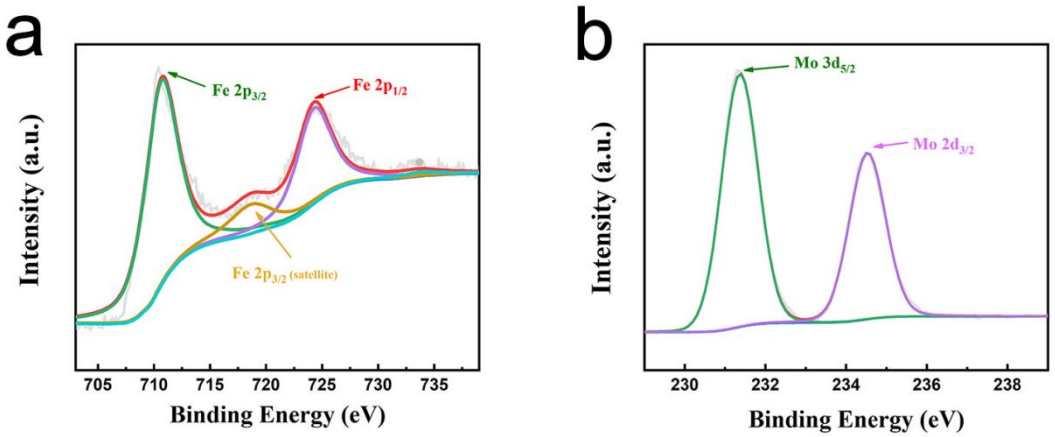


**Fig. S2** The XPS spectra of FMO-NPs in Fe 2p (a) and Mo 3d (b) region

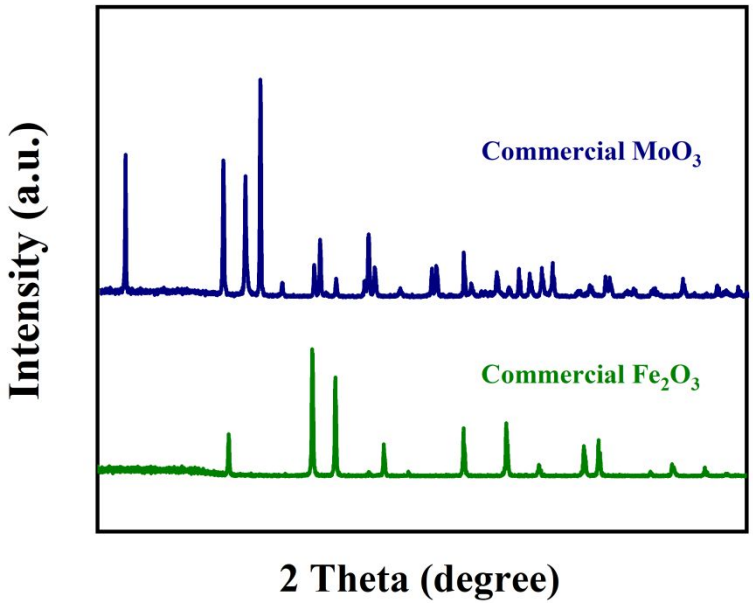


**Fig. S3.** XRD pattern of commercial $Fe_2O_3$ and commercial $MoO_3$

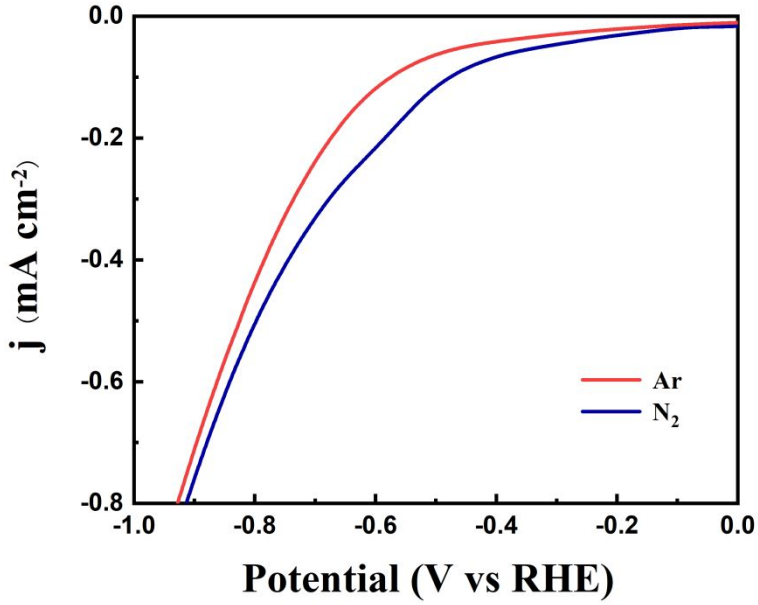


**Fig. S4.** LSV curves of FMO-NPs in Ar- and $N_2$-saturated 0.1M $Na_2SO_4$ with the scan rate of 5 mV/s.

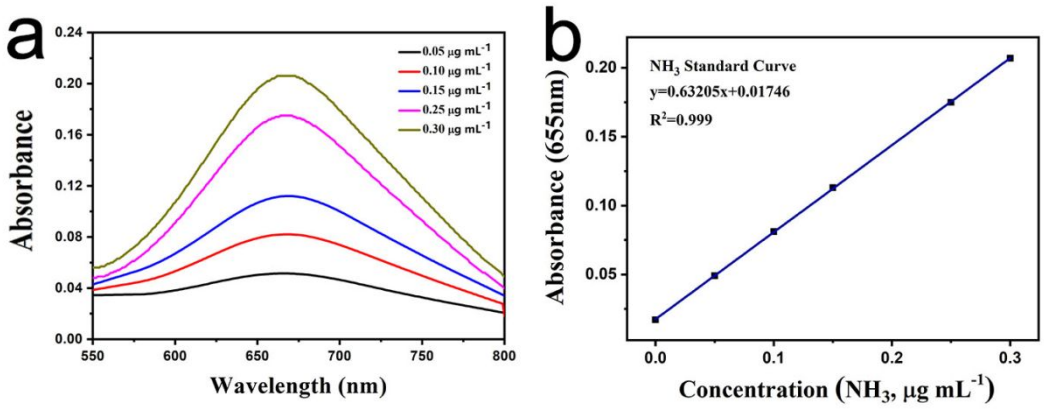


**Fig. S5.** (a) UV-Vis absorption spectra of indophenol assays with $NH_3$ after incubation for 2 h at room temperature 0.1M $Na_2SO_4$ electrolyte; (b) calibration curve used for estimation of $NH_3$ by $NH_3$ concentration.

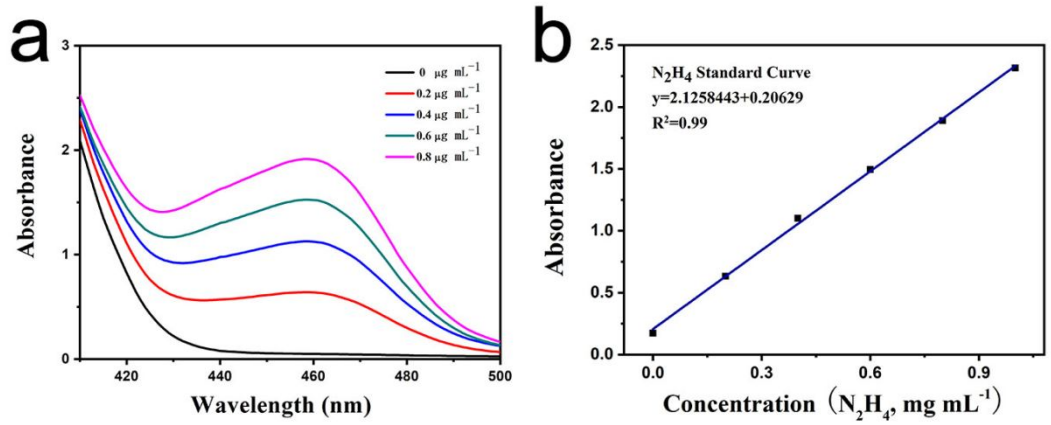


**Fig. S6.** (a) UV-Vis curves of various $N_2H_4$ concentrations after adding into chemical indicator by the method of Watt and Chrisp. (b) Calibration curve used for calculation of $N_2H_4$ concentrations.

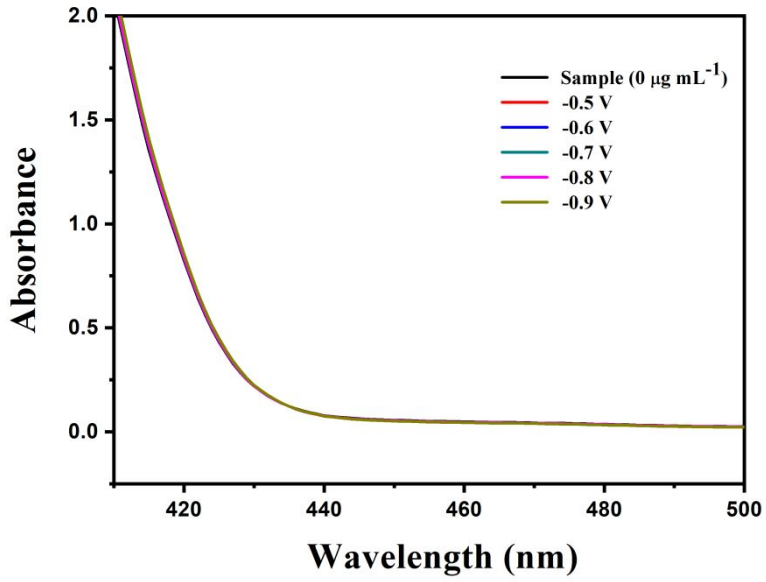


**Fig. S7.** UV-Vis absorption spectra of the electrolytes estimated by the method of Watt and Chrisp after electrolysis in $N_2$-saturated 0.1M $Na_2SO_4$ at a series of potentials for FMO-NPs.

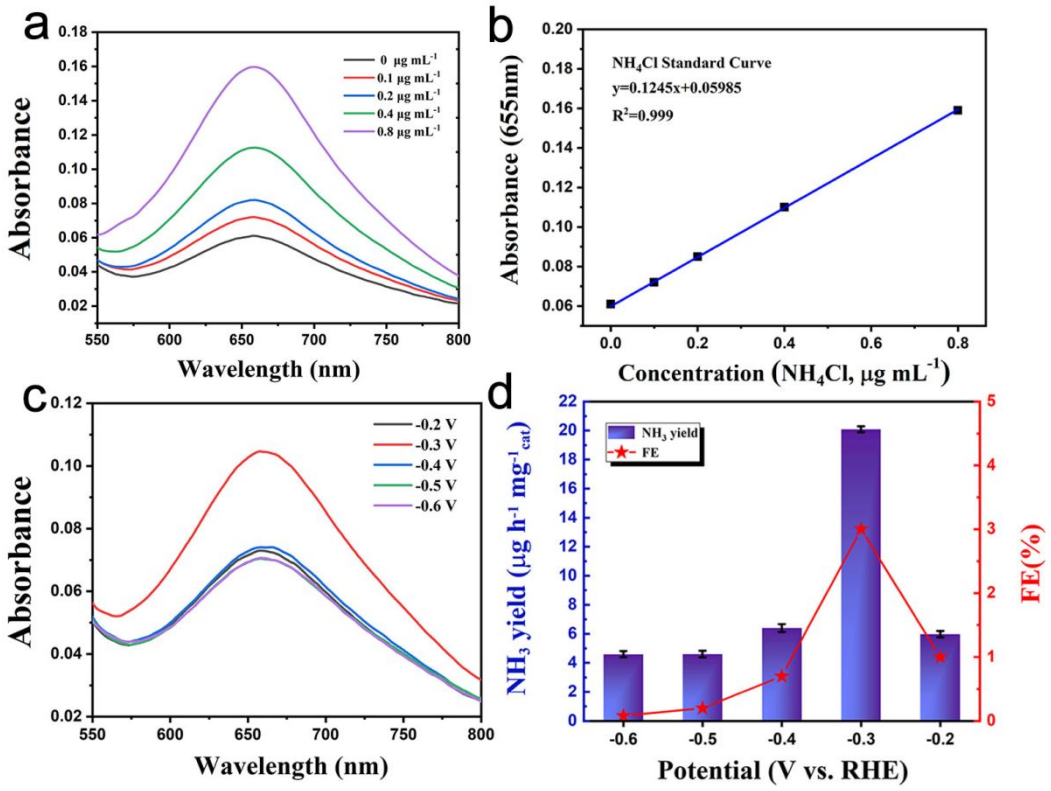


**Fig. S8.** (a) UV-Vis absorption spectra of indophenol assays with $NH_4Cl$ after incubation for 2 h at room temperature in 0.1M HCl electrolyte; (b) calibration curve used for estimation of $NH_3$ by $NH_4Cl$ concentration.(c) UV-Vis absorption spectra of the electrolytes stained with indophenol indicator at a series of potentials in 0.1M HCl electrolyte after electrolysis for 2 h. (d) $NH_3$ yields and FEs for FMO-NPs at corresponding potentials.

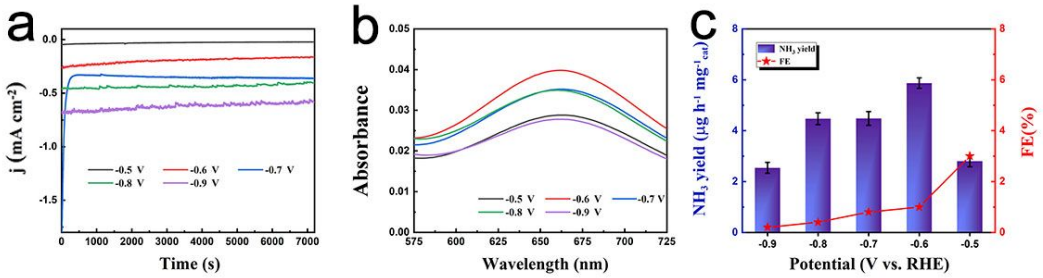


**Fig. S9.** (a) Time-dependent current density curves over commercial $Fe_2O_3$ at various potentials for 2 h in 0.1M $Na_2SO_4$. (b) UV-Vis absorption spectra of the electrolytes stained with indophenol indicator at a series of potentials after electrolysis for 1 h. (c) $NH_3$ yields and FEs for commercial $Fe_2O_3$ at corresponding potentials.

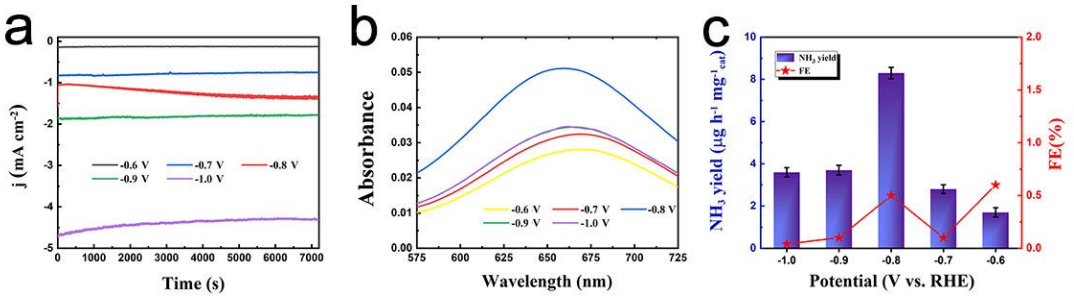


**Fig. S10.** (a) Time-dependent current density curves over commercial $MoO_3$ at various potentials for 2 h in 0.1M $Na_2SO_4$. (b) UV-Vis absorption spectra of the electrolytes stained with indophenol indicator at a series of potentials after electrolysis for 1 h. (c) $NH_3$ yields and FEs for commercial $MoO_3$ at corresponding potentials.

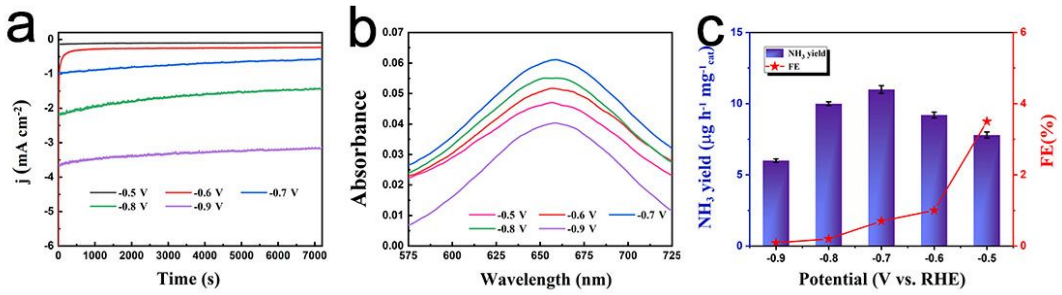


**Fig. S11.** (a) Time-dependent current density curves over mixture ($Fe_2O_3$ + $3MoO_3$) at various potentials for 2 h in 0.1M $Na_2SO_4$. (b) UV-Vis absorption spectra of the electrolytes stained with indophenol indicator at a series of potentials after electrolysis for 1 h. (c) $NH_3$ yields and FEs for mixture ($Fe_2O_3$ + $3MoO_3$) at corresponding potentials.

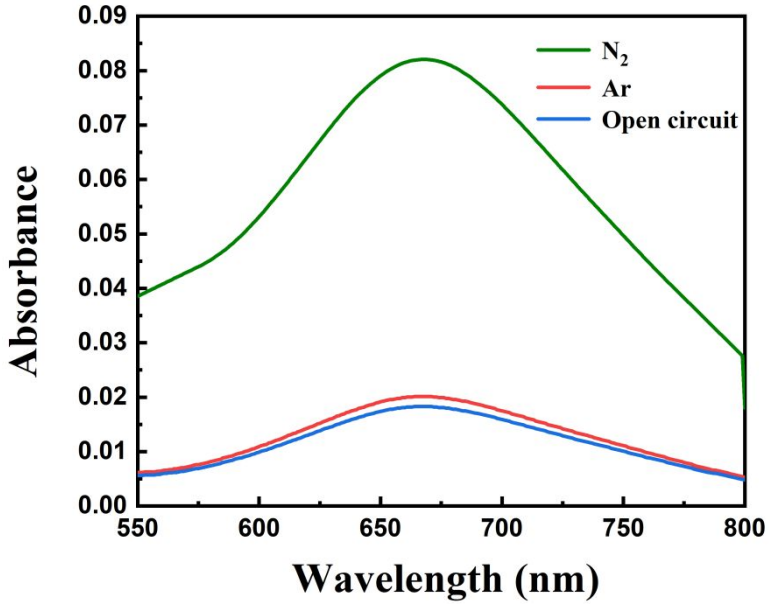


**Fig. S12.** UV-Vis absorption spectra of indophenol assays with the electrolytes under different condition.

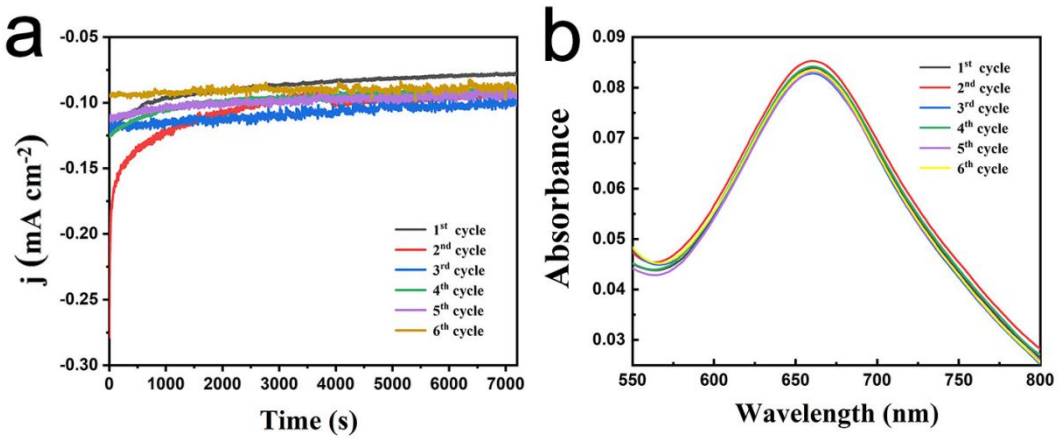


**Fig. S13.** (a) Time-dependent current density curves of FMO-NPs at –0.6 V for 6 cycles. (b) UV-Vis absorption spectra of the electrolytes stained with indophenol indicator after NRR electrolysis under different conditions for 6 cycles.

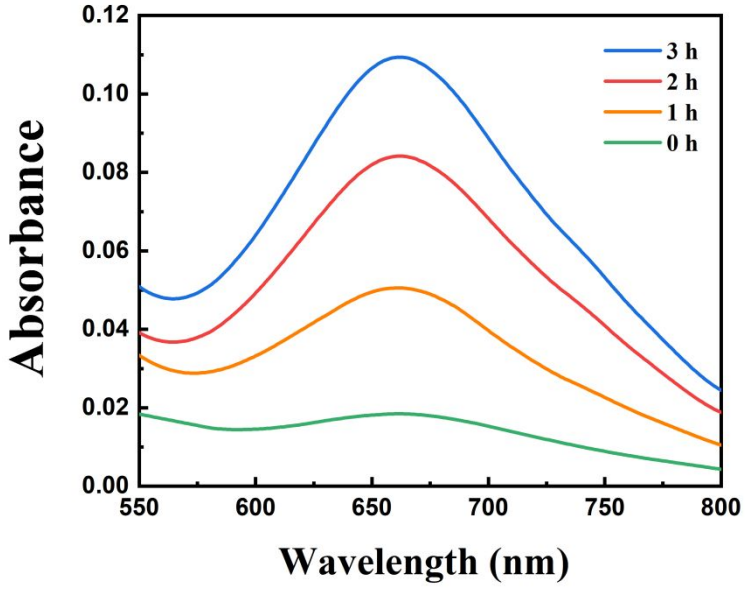


**Fig. S14.** UV-vis absorption spectra of indophenol assays with electrolyte after different electrolysis time (h) at room temperature.

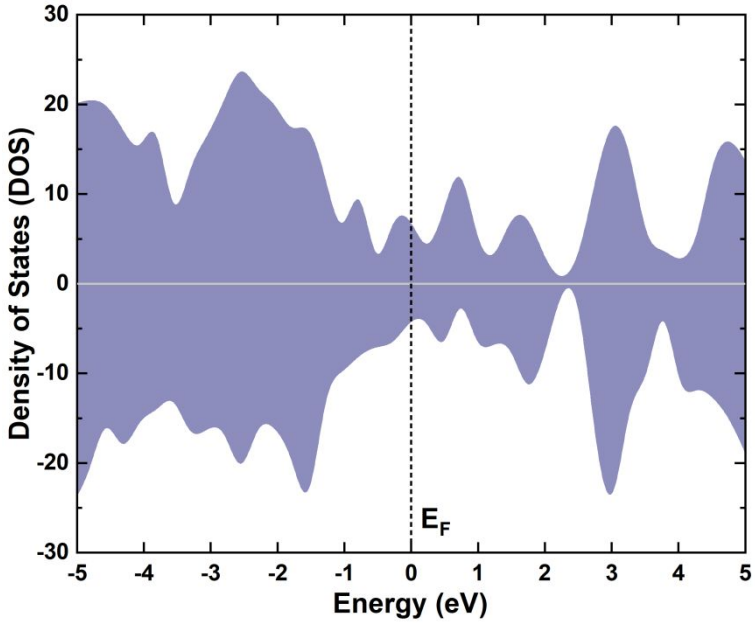


**Fig. S15.** Calculated density of states (DOS) of $Fe_2(MoO_4)_3$ (110) surface.

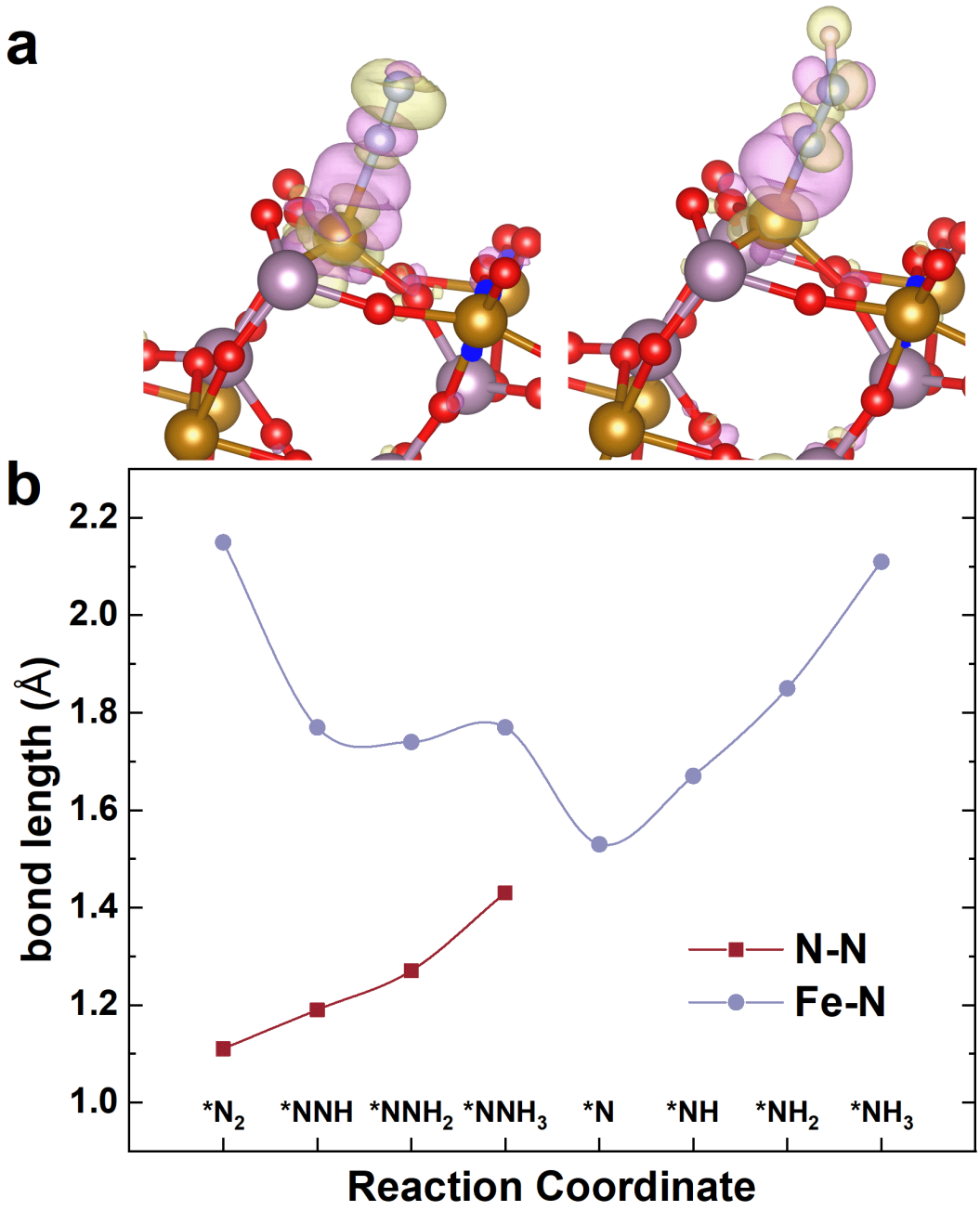


**Fig. S16.** (a) Calculated charge density difference of *$N_2$, *NNH. (b) Bond lengths of N-N, Fe-N through distal pathway.

**Table S1.** Calculated zero point energies and entropy of different adsorption species, where the * denotes the adsorption site. T was set as 300K.

| Adsorption Species | $E_{ZPE}$ (eV) | $T\Delta S$ (eV) |
|---|---|---|
| ***NN** | 0.22 | 0.22 |
| ***NNH** | 0.41 | 0.25 |
| ***HNNH** | 0.79 | 0.13 |
| ***$HNNH_2$** | 1.16 | 0.25 |
| ***$H_2NNH_2$** | 1.53 | 0.21 |
| ***$H_2NNH_3$** | 1.75 | 0.22 |
| ***$NH_2$** | 0.62 | 0.15 |
| ***$NH_3$** | 0.96 | 0.09 |

**Table S2.** Comparison of electrocatalytic $N_2$ reduction performance for FMO-NPs with other electrocatalysts under ambient conditions.

| **Catalyst** | **Electrolyte** | **$NH_3$ yield** | **FE%** | **Ref.** |
|---|---|---|---|---|
| **FMO-NPs** | **0.1M $Na_2SO_4$** | **18.16 μg $h^{-1}$ $mg^{-1}_{cat.}$** | **9.1** | **This work** |
| PEBCD/C | 0.1M $Li_2SO_4$ | 1.58 μg $h^{-1}$ $mg^{-1}_{cat.}$ | 2.85 | [1] |
| $La_2O_3$ | 0.1M $Na_2SO_4$ | 17.04 μg $h^{-1}$ $mg^{-1}_{cat.}$ | 4.76 | [2] |
| $Cr_{0.1}CeO_2$ | 0.1M HCl | 16.82 μg $h^{-1}$ $mg^{-1}_{cat.}$ | 3.84 | [3] |
| Bi NS | 0.1M $Na_2SO_4$ | 13.23 μg $h^{-1}$ $mg^{-1}_{cat.}$ | 10.46 | [4] |
| $TiO_2$/rGO | 0.1M $Na_2SO4$ | 15.13 μg $h^{-1}$ $mg^{-1}_{cat.}$ | 3.3 | [5] |
| $LaFeO_3$ | 2M KOH | 13.46 μg $h^{-1}$ $mg^{-1}_{cat.}$ | 1.99 | [6] |
| Pd/C | 0.1M PBS | 4.5 μg $h^{-1}$ $mg^{-1}_{cat.}$ | 8.2 | [7] |
| $Bi_4V_2O_{11}/CeO_2$ | 0.1M HCl | 23.21 μg $h^{-1}$ $mg^{-1}_{cat.}$ | 10.16 | [8] |
| $B_4C$ | 0.1M HCl | 26.57 μg $h^{-1}$ $mg^{-1}_{cat.}$ | 15.95 | [9] |
| CoP HNC | 1M KOH | 10.78 μg $h^{-1}$ $mg^{-1}_{cat.}$ | 7.36 | [10] |
| BNS | 0.1M $Na_2SO_4$ | 13.22 μg $h^{-1}$ $mg^{-1}_{cat.}$ | 4.04 | [11] |
| Pd-Co/CuO | 0.1M KOH | 10.04 $h^{-1}$ $mg^{-1}_{cat.}$ | 2.16 | [12] |
| N-doped porous carbon | 0.05M $H_2SO_4$ | 23.8 μg $h^{-1}$ $mg^{-1}_{cat.}$ | 1.42 | [13] |
| YSZ | 0.1M $Na_2SO_4$ | 10.84 μg $h^{-1}$ $mg^{-1}_{cat.}$ | 12.3 | [14] |
| Defect-Rich Bi | 0.2M $Na_2SO_4$ | 5.453 μg $h^{-1}$ $mg^{-1}_{cat.}$ | 11.68 | [15] |
| CuO/graphene | 0.1M HCl | $1.8 \times 10^{-10}$ mol $s^{-1}$ $cm^{-2}$ | 3.9 | [16] |
| PdRu TPs | 0.1M KCl | 37.23 μg $h^{-1}$ $mg^{-1}_{cat.}$ | 1.85 | [17] |

**Table S3.** Comparison of electrocatalytic $N_2$ reduction performance for FMO-NPs with other Fe-based and Mo-based electrocatalysts under ambient conditions.

| **Catalyst** | **Electrolyte** | **$NH_3$ yield** | **FE%** | **Ref.** |
|---|---|---|---|---|
| **FMO-NPs** | **0.1 M $Na_2SO_4$** | **18.16 μg $h^{-1}$ $mg^{-1}_{cat.}$** | **9.1** | **This work** |
| FeS@$MoS_2$/CFC | 0.1M KOH | 8.75 μg $h^{-1}$ $mg^{-1}_{cat.}$ | 2.96 | [18] |
| $MoS_2$ | 0.1M $Na_2SO_4$ | 8.08 × $10^{-11}$ mol $s^{-1}$ $cm^{-2}$ | 1.17 | [19] |
| $MoO_3$ | 0.1M HCl | 4.80×$10^{-10}$ mol $s^{-1}$ $cm^{-2}$ | 1.9 | [20] |
| $MoO_2$/RGO | 0.1M $Na_2SO_4$ | 37.4 μg $h^{-1}$ $mg^{-1}_{cat.}$ | 6.6 | [21] |
| γ -$Fe_2O_3$ | 0.1M KOH | 12.5 nmol $h^{-1}$ $mg^{-1}$ | 1.9 | [22] |
| $Fe_3O_4$/Ti | 0.1M $Na_2SO_4$ | 5.6 × $10^{-11}$ mol $s^{-1}$ $cm^{-2}$ | 2.6 | [23] |
| $Fe_2O_3$ nanorods | 0.1M $Na_2SO_4$ | 15.9 μg $h^{-1}$ $mg^{-1}_{cat.}$ | 0.94 | [24] |
| $Fe_3S_4$ | 0.1M HCl | 75.4 μg $h^{-1}$ $mg^{-1}_{cat.}$ | 6.45 | [25] |

## References


1 Chen, G.; Cao, X.; Wu, S.; Zeng, X.; Ding, L.; Zhu, M.; Wang, H. Ammonia Electrosynthesis with High Selectivity under Ambient Conditions via a $Li^+$ Incorporation Strategy. *J. Am. Chem. Soc.* **2017**, *139*, 9771–9774.

2 Xu, B.; Liu, C.; Qiu, B.; Liu, Q.; Sun, P.; Cui, W.; Wu, Y.; Xiong, X. $La_2O_3$ Nanoplate: An Efficient Electrocatalyst for Artificial $N_2$ Fixation to $NH_3$ with Excellent Selectivity at Ambient Condition. *Electrochim Acta* **2018**, *298*, 106-111.

3 Xie, H.; Wang, B.; Geng, Q.; Xing, Z.; Wang, W.; Chen, Y.; Ji, L.; Chang, L.; Wang, M.; Mao, J. Oxygen Vacancies of Cr-Doped $CeO_2$ Nanorods That Efficiently Enhance the Performance of Electrocatalytic $N_2$ Fixation to $NH_3$ under Ambient Conditions. *Inorg. Chem.* **2019**, *58*, 5423-5427.

4 Li, L.; Tang, C.; Xia, B.; Jin, H.; Zheng, Y.; Qiao, S. Two-Dimensional Mosaic Bismuth Nanosheets for Highly Selective Ambient Electrocatalytic Nitrogen Reduction. *ACS Catal.* **2019**, *9*, 2902–2908.

5 Zhang, X.; Liu, Q.; Shi, X.; Asiri, A. M.; Luo, Y.; Sun, X.; Li, T. $TiO_2$ Nanoparticles–reduced Graphene Oxide Hybrid: An Efficient and Durable Electrocatalyst toward Artificial $N_2$ Fixation to $NH_3$ under Ambient Conditions. *J. Mater. Chem. A* **2018**, *6*, 17303–17306.

6 Zhang, S.; Duan, G.; Qiao, L.; Tang, Y.; Chen, Y.; Sun, Y.; Wan, P.; Zhang, S. Electrochemical Ammonia Synthesis from $N_2$ and $H_2O$ Catalyzed by Doped $LaFeO_3$ Perovskite under Mild Conditions. *Ind. Eng. Chem. Res.* **2019**, *58*, 8935–8939.

7 Wang, J.; Yu, L.; Hu, L.; Chen, G.; Xin, H.; Feng, X. Ambient Ammonia Synthesis via Palladium-catalyzed Electrohydrogenation of Dinitrogen at Low Overpotential. *Nat. Commun.* **2018**, *9*, 1795.

8 Lv, C.; Yan, C.; Chen, G.; Ding, Y.; Sun, J.; Zhou, Y.; Yu, G. An Amorphous Noble‐Metal‐Free Electrocatalyst that Enables Nitrogen Fixation under Ambient Conditions. *Angew. Chem., Int. Ed*. **2018**, *57*, 6073–6076.

9 Qiu, W.; Xie, X.; Qiu, J.; Fang, W.; Liang, R.; Ren, X.; Ji, X.; Cui, G.; Asiri, A. M.; Cui, G.; Tang, B.; Sun, X. High-performance Artificial Nitrogen Fixation at Ambient Conditions Using A Metal-free Electrocatalyst. *Nat. Commun.* **2018**, *9*, 3485.

10 Guo, W.; Liang, Z.; Zhao, J.; Zhu, B.; Cai, K.; Zou, R.; Xu, Q. Hierarchical Cobalt Phosphide Hollow Nanocages toward Electrocatalytic Ammonia Synthesis under Ambient Pressure and Room Temperature. *Small Methods* **2018**, *2*, 1800204.

11 Zhang, X.; Wu, T.; Wang, H.; Zhao, R.; Chen, H.; Wang, T.; Wei, P.; Luo, Y.; Zhang, Y.; Sun, X. Boron Nanosheet: An Elemental Two-Dimensional (2D) Material for Ambient Electrocatalytic $N_2$-to-$NH_3$ Fixation in Neutral Media. *ACS Catal.* **2019**, *9*, 4609–4615.

12 Fu, W.; Cao, Y.; Feng, Q.; Smith, W. R.; Dong, P.; Ye, M.; Shen, J. Pd–Co Nanoalloys Nested on CuO Nanosheets for Efficient Electrocatalytic $N_2$ Reduction and Room-temperature Suzuki–Miyaura Coupling Reaction. *Nanoscale* **2019**, *11*, 1379–1385.

13 Liu, Y.; Su, Y.; Quan, X.; Fan, X.; Chen, S.; Yu, H.; Zhao, H.; Zhang, Y.; Zhao, J. Facile Ammonia Synthesis from Electrocatalytic $N_2$ Reduction

under Ambient Conditions on N-Doped Porous Carbon. *ACS Catal.* **2018**, *8*, 1186–1191.

14 Xian, H.; Wang, Q.; Yu, G.; Wang, H.; Li, Y.; Wang, Y.; Li, T. Electrochemical Synthesis of Ammonia by Zirconia-based Catalysts at Ambient Conditions. *Appl. Catal. A-Gen.* **2019**, *581*, 116–122.

15 Wang, Y.; Shi, M.; Bao, D.; Meng, F.; Zhang, Q.; Zhou, Y.; Liu, K.; Zhang, Y.; Wang, J.; Wang, J.; Chen, Z.; Liu, D.; Jiang, Z.; Luo, M.; Gu, L.; Zhang, Q.; Cao, X.; Yao, Y.; Shao, M.; Zhang, Y.; Zhang, X.; Chen, J.; Yan, J.; Jiang, Q. Generating Defect‐Rich Bismuth for Enhancing Rate of Nitrogen Electroreduction to Ammonia. *Angew. Chem*, *Int. Ed.* **2019**, *58*, 9464–9469.

16 Wang, F.; Liu, Y.; Zhang, H.; Chu, K. CuO/graphene Nanocomposite for Nitrogen Reduction Reaction. *Chem. Cat. Chem.* **2019**, *11*, 1441–1447.

17 Wang, H.; Li, Y.; Li, C.; Deng, K.; Wang, Z.; Xu, Y.; Li, X.; Xue, H.; Wang, L. One-pot Synthesis of Bi-metallic PdRu Tripods as An Efficient Catalyst for Electrocatalytic Nitrogen Reduction to Ammonia. *J. Mater. Chem. A* **2019**, *7*, 801–805.

18 Guo, Y.; Ya, Z.; Timmer, B. J. J.; Sheng, X.; Fan, L.; Li, Y.; Zhang, F.; Sun, L. Boosting Nitrogen Reduction Reaction by Bio-inspired FeMoS Containing Hybrid Electrocatalyst over A Wide PH Range. *Nano. Energy* **2019**, *62*, 282–288.

19 Zhang, L.; Ji, X.; Ren, X.; Ma, Y.; Shi, X.; Tian, Z.; Asiri, A. M.; Chen, L.; Tang, B.; Sun, X. Electrochemical Ammonia Synthesis via Nitrogen Reduction Reaction on MoS2 Catalyst: Theoretical and Experimental Studies. *Adv. Mater.* **2018**, *30*, 1800191.

20 Han, J.; Ji, X.; Ren, X.; Cui, G.; Li, L.; Xie, F.; Wang, H.; Li, B.; Sun, X. $MoO_3$ Nanosheets for Efficient Electrocatalytic $N_2$ Fxation to $NH_3$. *J. Mater. Chem. A* **2018** *6* 12974–12977.

21 Wang, J.; Liu, Y.; Zhang, H.; Huang, D.; Chu, K. Ambient Electrocatalytic Nitrogen Reduction on A $MoO_2$/graphene Hybrid: Experimental and DFT Studies. *Catal. Sci. Technol.* **2019,** DOI**:** 10.1039/C9CY00907H.

22 Kong, J.; Lim, A.; Yoon, C.; Jang, J.; Ham, H. C.; Han, J.; Nam, S.; Kim, D.; Sung, Y. E.; Choi, J.; Park, H. S. Electrocatalytic Nitrogen Reduction to Ammonia by $Fe_2O_3$ Nanorod Array on Carbon Cloth. *ACS. Sustainable. Chem. Eng.* **2017**, *5*, 10986–10996.

23 Liu, Q.; Zhang, X.; Zhang, B.; Luo, Y.; Cui, G.; Xie, F.; Sun, X. Ambient $N_2$ Fixation to $NH_3$ Electrocatalyzed by Spinel $Fe_3O_4$ nanorod. *Nanoscale* **2018**, *10*, 14386–14389.

24 Xiang, X.; Wang, Z.; Shi, X.; Fan, M.; Sun, X. Ammonia Synthesis from Electrocatalytic $N_2$ Reduction under Ambient Conditions by $Fe_2O_3$ Nanorods. *Chem. Cat. Chem.* **2018**, *20,* 4530–4535.

25 Zhao, X.; Lan, X.; Yu, D.; Fu, H.; Liu, Z.; Mu, T. Deep Eutectic-solvothermal Synthesis of Nanostructured $Fe_3S_4$ for Electrochemical $N_2$ Fixation under Ambient Conditions. *Chem. Commun.* **2018**, *54,* 13010.